Research in Astronomy and Astrophysics, 22:075002 (11pp), 2022 July https://doi.org/10.1088/1674-4527/ac6e59

A Detailed Study of Mode Changing and Modulation of PSR B1237+25 with FAST

Zheng-Wu Wang[1,2], Mao Yuan[1,2], Lin Wang[1,2], Cheng-Min Zhang[1], and Bo Peng[1]
[1] CAS Key Laboratory of FAST, National Astronomical Observatories, Chinese Academy of Sciences, Beijing 100101, China; pb@bao.ac.cn
[2] School of Astronomy and Space Science, University of Chinese Academy of Sciences, Beijing 100049, China
Received 2022 February 24; revised 2022 April 10; accepted 2022 April 19; published 2022 June 14

Abstract

PSR B1237+25, whose mean pulse profile has five components, is a well-known star to study pulsar emission geometries. We conducted mode changing and modulation analysis on this pulsar using FAST data at 1.25 GHz with a bandwidth of 400 MHz. We observed and identified three emission modes of this pulsar: a quiet normal mode that has little or no core activity with distinctive 2.8-period subpulse modulation on its outer cone, a flare normal mode in which the core is highly active and an abnormal mode in which the core is active and the last component is weak. We found that the core activity cuts off the position angle traverse in flare normal mode and leads to a position angle jumping in abnormal mode. We also found that there exists a quasi-periodical modulation on the outer conal components. Such modulation shows an irregular wave-like pattern, and has a weak correlation with the core component. We discuss the likely origin of such a modulation, and argue that this modulation can be interpreted as precession of the emission cones around the magnetic axis.

Key words: (stars:) pulsars: individual (PSR B1237+25) – radiation mechanisms: non-thermal – magnetic fields – polarization

1. Introduction

Unlike the integrated profile of radio pulsars demonstrating the stable feature of emission properties, individual pulse series contain the information on emission dynamics (Hankins & Wright 1980). Some theories have been built to explain the rich phenomena such as nulling, drifting, and modulation. A widely accepted model to explain the drifting subpulses is the carousel-type model (Ruderman & Sutherland 1975). It suggests that a drifting subpulse, which is recognized as a phase modulation of the pulse profile, is caused by sparks circulating around the magnetic axis in the inner gap near the surface of the neutron star. A large number of drifting subpulses has been identified, providing strong support to the carousel-type model.

The Ruderman–Sutherland (RS) model considers only the curvature radiation process in a pulsar's magnetosphere, therefore it is an oversimplified model. Various common phenomena, like the erratic drifting rate and direction, the conversion between different drifting modes (Wen et al. 2016; Basu et al. 2019) and the core emission component, are still unable to be understood well, though numerous attempts have been made to face these challenges. van Horn (1980) explained the quasi-periodic oscillation of micropulse and subpulse drifting by including the influence of torsional oscillations of neutron star crusts. The inverse Compton scattering (ICS) model was proposed by Qiao & Lin (1998) and Xu et al. (2000), which includes the scattering cross-section of the high energy particles that are emitted from the inner gap. This model provides good interpretations of the phenomena such as the core emission component, the different emission heights for inner and outer components, and the aberration and retardation effects. Some researches have been done to explain the detailed problems such as "bi-drifting" (Qiao et al. 2004; Szary & van Leeuwen 2017), but there are still some questions, like the origin of orthogonal-polarization-mode (hereafter OPM), that need to be further investigated.

PSR B1237+25 has five emission components, generally used as an example to study pulsar emission geometry. This bright pulsar has a dispersion measure of 9.25 pc cm^{-3} and a period of 1.38 s. Its five emission components are usually caused by two emission cones and one central emission core (Lyne & Manchester 1988). The central position angle (PA) has a sweeping rate of nearly 180°/deg in the core region, indicating that it has a magnetic axis close to the line of sight. This scenario provides us an extraordinary opportunity to observe its magnetic polar cap and study the radio emission dynamics. Emission state transition between two distinctive emission modes has been observed (Backer 1970a, 1970b, 1970c, 1973): the normal mode and the abnormal mode. Srostlik & Rankin (2005) further divided the normal mode into a quiet normal mode in which core activity is relatively weak and a flare normal mode where the core is highly active. These emission modes manifest different properties that one can use to estimate the height of emission and verify the geometric

models of pulsars' polar caps (Rankin 1983, 1986, 1990; Radhakrishnan & Rankin 1990). It also has a regular $2.8P$ cycle^{-1} subpulse modulation in the normal mode, but such a modulation reveals little information on any drifting property (Srostlik & Rankin 2005).

With the establishment of the Five-hundred-meter Aperture Spherical radio Telescope (FAST, Nan 2009), astronomers can observe pulsars with unprecedented sensitivity. The much deeper observations can provide us with new phenomena which could pose challenges to existing emission models. This gives us an opportunity to understand the nature of pulsar emission mechanisms and dynamics.

In this paper, we present an analysis of PSR B1237+25 through its integrated pulse profiles and subpulse modulation properties. Section 2 describes our observation settings and data reduction procedures. We present the integrated profiles in Section 3, and the nulling and modulation are analyzed in Section 4. We discuss the emission geometry and the newly found irregular modulation phenomenon observed with FAST in Section 5, and summarize the results in Section 6.

2. Observation and Data Reduction

FAST is located in Pingtang County, Guizhou Province of China and was completed in September 2016. It is operated by National Astronomical Observatories, Chinese Academy of Science (NAOC). FAST has an aperture efficiency of 0.63 at 1.4 GHz and a system temperature less than 25 K (Jiang et al. 2020). A 19-beam receiver has been used since 2018, which has a frequency bandwidth of 1050–1450 MHz.

We observed PSR B1237+25 with an integration time of 1 hr using the 19-beam receiver of FAST in November 2019. During the observation, the data were sampled and digitized using Reconfigurable Open Architecture Computing Hardware 2 (ROACH2) and recorded in the format of 8 bit PSRFITS files. The data sets have 4096 channels which result in a channel bandwidth of 122 kHz. The sampling time of the data is 49 μs. Full Stokes parameters were recorded in the data. Before the observation, the telescope was pointed to an off-source region, and a signal from a noise diode with a period of 0.2 s and temperature of 1.2 K was injected for 5 minutes. The off-source data were recorded in the same format as the on-source data.

To accelerate the processing, we use the DSPSR software (van Straten & Bailes 2011) to divide the initial data into single pulses according to the period. The data were folded into 2048 bins, resulting in a longitude resolution of $0^{\circ}.176$. Then we eliminated the radio frequency interference using the pulsar software PSRCHIVE (Hotan et al. 2004) automatically, and the Stokes parameters were corrected for dispersion and interstellar Faraday rotation. To further visualize the data, we utilized PSRCHIVE to compress the single pulses in the frequency dimension, and the pulses were extracted to a text file to be further processed manually. The integrated profile can be acquired by averaging the single pulses in the sequence dimension.

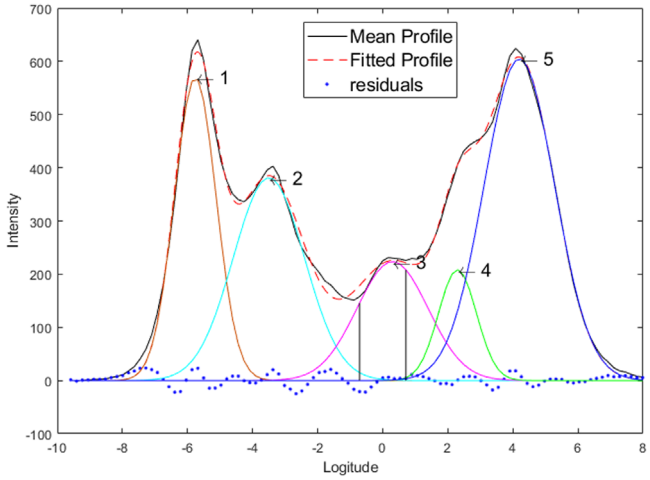

Figure 1. The integrated profile and the five component Gaussian decomposition of PSR B1237+25. The core component is labeled 3 in the figure. The FWHM of the core is about 2.3 degrees. The intensity in the core region marked with gray lines was counted to identify the two normal modes. The marked region has a width of 1.5σ with respect to the core Gaussian component, and was moved leftward slightly to avoid the influence from the fourth component.

We obtained 2605 single pulses in this observation. By averaging all subpulses, we gathered the integrated profile with signal to noise ratio (SNR) over 7600. We applied a Gaussian decomposition analysis to the integrated profile to find out the position of each component (Figure 1). The single-pulse data were then deduced by an integrated profile, and displayed in a pulse-sequence (PS) diagram, to identify the different modes (Figure 2). To avoid the influence of the scintillation effect, the pulse sequence is divided into several parts such that in each part the influence of scintillation is acceptable. The pulses in which the intensity in the 0.62–0.64 phase range is enhanced and the intensity in the 0.64–0.65 phase range is weakened were recognized as abnormal mode. We gathered 169 abnormal mode pulses in this observation. The identification of flare normal pulses and quiet normal pulses is difficult, because their outer cones' behavior is similar. We then used the intensity distribution of the core to distinguish the two normal modes, for the core activity dominates the main difference between the two normal modes (Figure 3). To avoid the influence from the fourth component, the intensities in the core region that have a width of 1.5σ were counted. About one quarter of pulses were recognized as the flare normal mode, and the rest were recognized as the quiet normal mode.

3. Integrated Profile

As displayed in Figure 4, the integrated profile of the whole observation from pulsar B1237+25 presents five typical

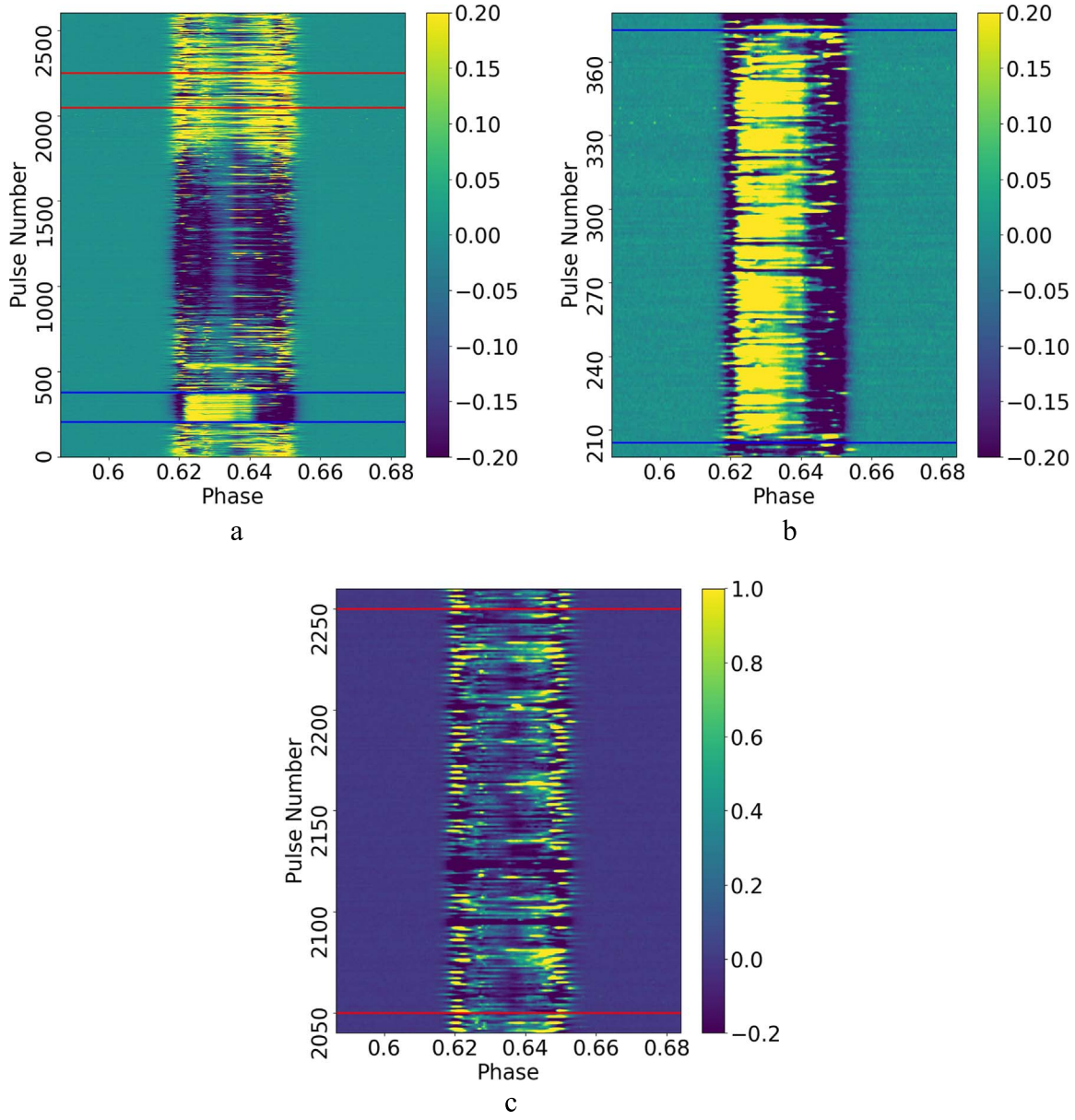

Figure 2. The PS diagram of the whole observation (a), and abnormal mode (b) and normal mode (c) pulses from PSR B1237+25. The observation was conducted by FAST in November 2019. All of the pulses were deduced by an integrated profile to make the abnormal mode clearer in the diagram. The dark region in the middle of the pulse sequence (a) was caused by interstellar scintillation. The abnormal mode (b) can be identified easily in the PS diagram. (c) Part of the normal mode pulses. The bright peaks on both edges of the normal mode are the 2.8-period modulated pulses. It is worth noticing that those peaks are "drifting" in the longitude direction, forming a quasi-periodic "wave-like" pattern.

emission components with central PA traverse. This integrated profile consists of 2605 pulses, including 6.5% abnormal mode pulses, and 93.5% normal mode pulses where both the flare normal mode and the quiet normal mode are included. In the figure, the PA sweeps downward 180°, and owns a width of about 1° in the longitude window. Due to the aberration and retardation, components 4 and 5 are closer than components 1 and 2. The profile is generally symmetrical, while components 1 and 2 are slightly stronger than components 4 and 5. Components 2 and 4 show a relatively higher degree of polarization than the outer two components. It has been noticed that the left side of component 1 and the right side of component 5, as well as part of the core component, have a small jump in PA. The core region of the integrated profile is depolarized.

Figure 5 presents the integrated profile of the quiet normal mode. The appearance of the profile in this mode is almost

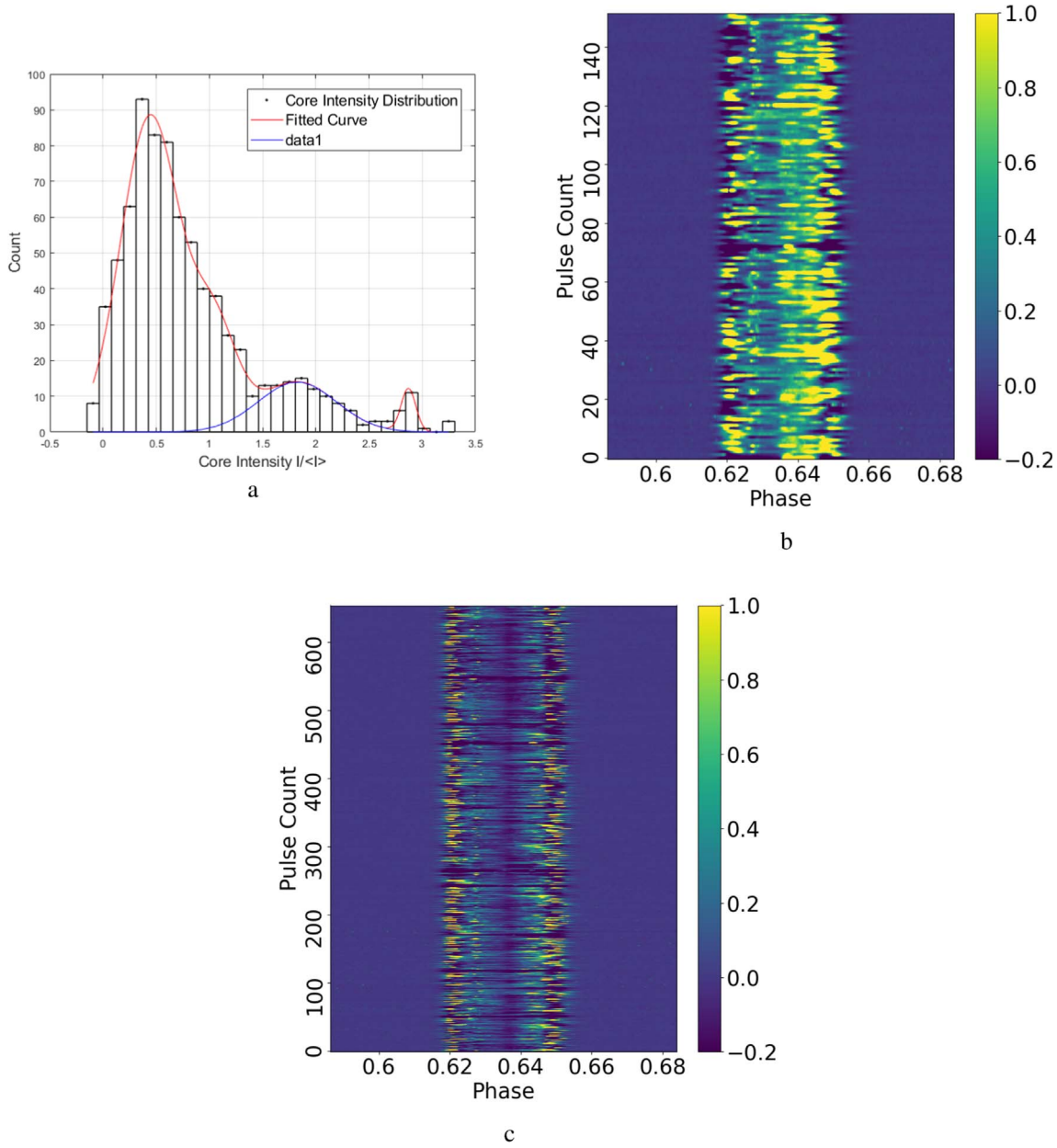

Figure 3. The intensity distribution of the core in pulse numbers 1800–2600 (a), and the extracted PS for the flare normal mode (b) and quiet normal mode (c). We chose this set of pulse numbers to avoid the influence of interstellar scintillation. (a) The intensity distribution of the core region marked in Figure 1. The intensity of the core is normalized and fitted with a Gaussian function. The pulses for which the core intensity exceeds 1.4 times the mean intensity form a Gaussian distribution, and can be used to separate the two normal modes. (b) The PS diagram of flare normal mode extracted from B1237+25 in pulse numbers 1800–2600. (c) The PS diagram of quiet normal mode extracted from B1237+25. Compared with the flare normal mode, the core activity in this mode is quiet.

indistinguishable from the integrated profile of the whole observation, while the only difference is the core component which almost vanishes. This is because most of the pulses in this observation are in the quiet normal mode. This emission mode contains little or no core activity, leaving a broad flat region in the center. It is difficult to recognize the direction of circular polarization because the circular polarization component is too weak. This is different from the low-frequency observations in which the core region posed a slight anti-symmetrical circular signature (Srostlik & Rankin 2005). Compared with the lower frequency observations, the two emission cones in our observation at L band are more compact. The 180° PA traverse is usually disrupted in the total profile, but can be seen clearly in this mode.

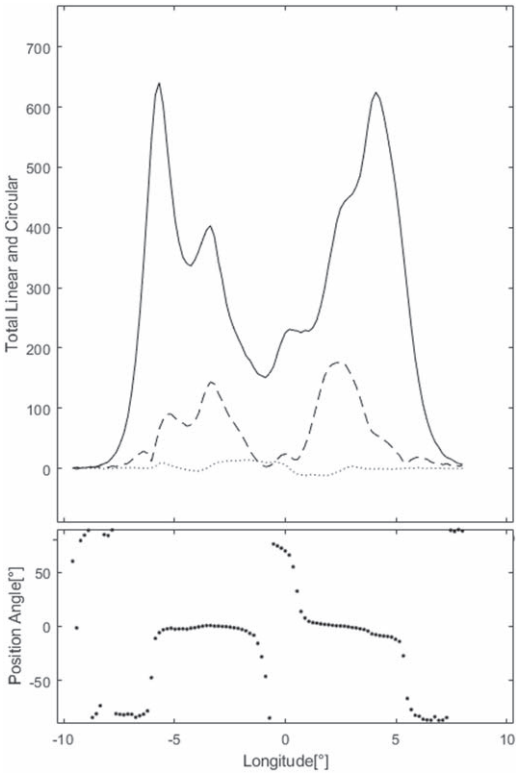

Figure 4. Integrated profile of total pulses of PSR B1237+25. The total intensity I, linear polarization $L = [(Q^2 + U^2)^{1/2}]$ and circular polarization V are plotted in the upper panel (solid, dashed and dotted curves, respectively), and the PA ($\chi = \frac{1}{2}\tan^{-1}U/Q$) is plotted in the bottom panel. The intensity of the vertical axis in the upper panel is in an arbitrary unit.

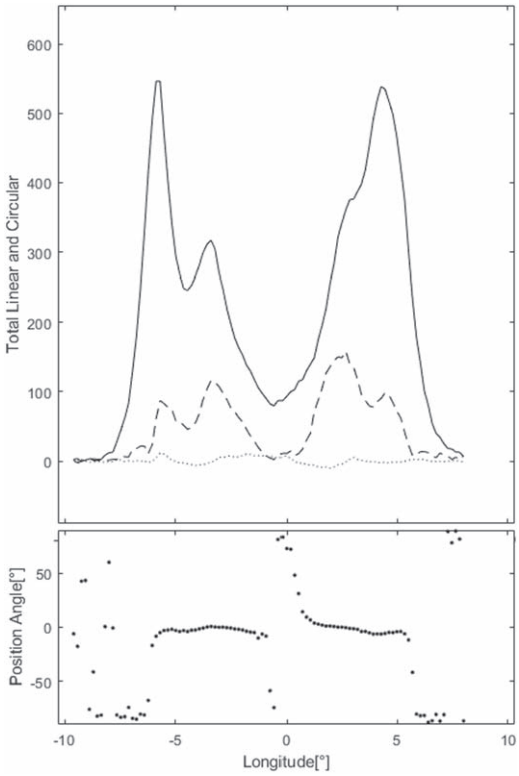

Figure 5. Integrated profile of quiet normal mode of PSR B1237+25. The pulses were recognized by visual inspection of the PS diagram. The core was quiet and the small PA jump in the center vanishes. The left side of component 1 and the right side of component 5 have PA orthogonal to the inner component.

Figure 6 demonstrates the profile of a flare normal mode. The flare normal mode is usually recognized as the core active pulses in a PS diagram, with intervals in a quiet normal mode having several pulses. In this mode, the core component is highly active, but less polarized. The anti-symmetrical circular polarization associated with the core component becomes much more evident, and component 5 is obviously enhanced while components 1, 2 and 4 are almost unaltered. The central PA traverse was cut off by the active core, and became a small positive protuberance.

Figure 7 displays the integrated profile of the abnormal mode. This mode can be easily distinguished from the PS diagram by its tight and narrow features. Components 1 and 2 seem to be merged in the PS diagram. The emission peaks in abnormal mode are relatively obscured compared with other emission states. The position of components 4 and 5 seems to be moved forward slightly, and component 4 is almost buried in the integrated profile, only leaving a flat polarization signature in the lower plot. The second component as well as its linear polarization seems to be enhanced in this mode, and components 4 and 5 are clearly weakened. A PA jump arises in the core region, and lasts for about $1^{\circ}.8$ in the longitude window. The PA jump in component 5 is enhanced too, and shifts to an earlier phase of about 1 degree. It has been noticed that the abnormal mode displays a similar core and conal component behavior to another five-component pulsar B1737+13 (Force & Rankin 2010), where a PA jump in components 1 and 5 was observed, along with a highly active core. Several pulsars that have abnormal events also show that component 5 can shift to an earlier phase (Force & Rankin 2010; Yu et al. 2019), indicating that they may have similar mechanisms. The width of this mode is about 1° narrower than the normal mode. The abnormal mode occasionally appears in the normal mode with several pulses, but can also shift to a longer period that lasts for hundred pulses.

4. Nulling Fraction and Subpulse Modulation

Nulling is a common phenomenon in pulsars (Backer 1970a), which can be identified from intensity histograms. The intensities of pulsars can often be fitted by a normal or log-normal distribution. Figure 8(a) demonstrates the normalized intensity distribution of this pulsar. The scintillation effect of the interstellar medium was ignored because it influences the

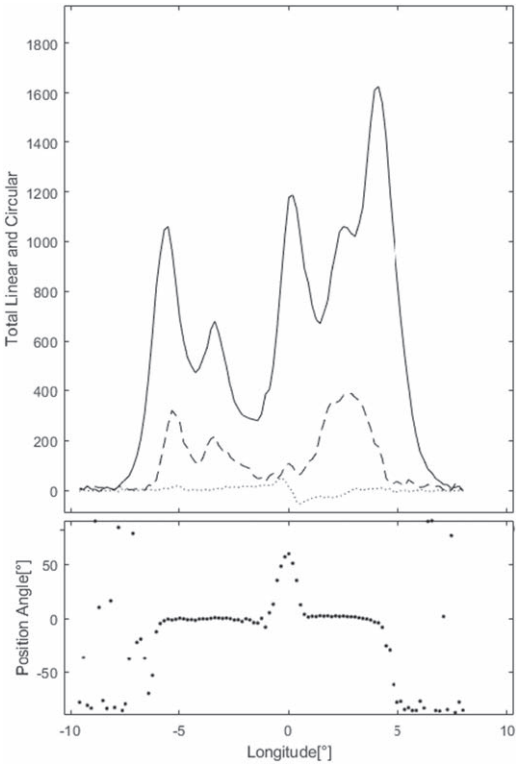

Figure 6. Integrated profile of flare normal mode of PSR B1237+25. Comparing with the quiet normal mode, component 5 in this mode is strongly enhanced. The PA traverse in the center changed and the PA jump in the trailing region shifted to an earlier phase.

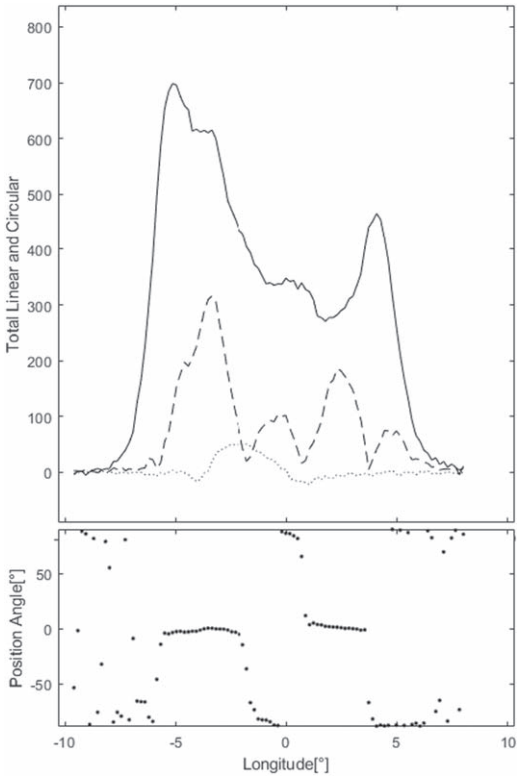

Figure 7. Integrated profile of abnormal mode, consisting of 169 abnormal pulses of PSR B1237+25. The emission components become blurry, and component 5, as well as the core component, is dominated by a PA orthogonal to the inner conal components. The center PA demonstrates continuous jumping, but was cut off by the limit of display.

distribution slightly. In the early study of PSR B1237+25 (Smith et al. 2013), approximately 5.2% of pulses were found to be "nulls". We identified 138 "null" pulses by taking a threshold of mean intensity of 0.3 $<I>$, giving a null fraction of 5.3%. PSR B1237+25 has also been reported to exhibit pseudo nulls (Maan & Deshpande 2014). The pseudo nulls will appear when the sightline cut through the minima of the carousel rather than the emission process stops (Herfindal & Rankin 2007). Those nulls usually last for only one period, because the chance of the sightline crossing the minima of two emission cones is too small.

In earlier studies, the pulsar B1237+25 has been reported to have a distinct 2.8-period subpulse modulation on its outer cones in the quiet normal mode (Backer 1970a, 1973), with quasi-periodic alternation of 5-15 short pulses in the flare normal mode and longer quiet normal mode of 60-80 pulses. Such 2.8-period modulation is easily identified from our PS diagram. However, we further noticed that the outer cone presents a quasi-periodic intensity modulation at its edge (Figure 9). The two outer cones show a "wave-like" appearance in the vertical direction of the PS diagram, and those components seem to be interacting with the core region. A similar pattern has been recognized as "diffused drifting" modulation (PSR B1737+13, Force & Rankin (2010), PSR J2048-1616, Wang et al. 2021). The length of this new modulation we observed is about 20 pulses, but can sometimes shift to a longer length of over 40 pulses. The shape of the "wave" in the PS diagram is discontinuous, and the trough of the wave in components 1 and 5 is generally asynchronous. Flare normal mode sometimes occurs around the inner side of the trough of the wave. The two inner cones are relatively stable, and show no obvious longitude-direction modulation properties. The abnormal mode also exhibits some subtle traces of modulation, but they are difficult to extract. Figure 10 is the longitude resolved fluctuation spectra of the normal mode.

5. Discussion

5.1. The Emission and Core Geometry

The width of the core component is always interesting as it reflects the geometry of radio pulsars (Gupta & Gangadhara 2003). It is actually difficult to measure the core width in an integrated profile for PSR B1237+25 because the core is weak and flat, appearing as two blurry weak components, hence we can only give a rough estimate of about $2\overset{\circ}{.}3$. This is consistent

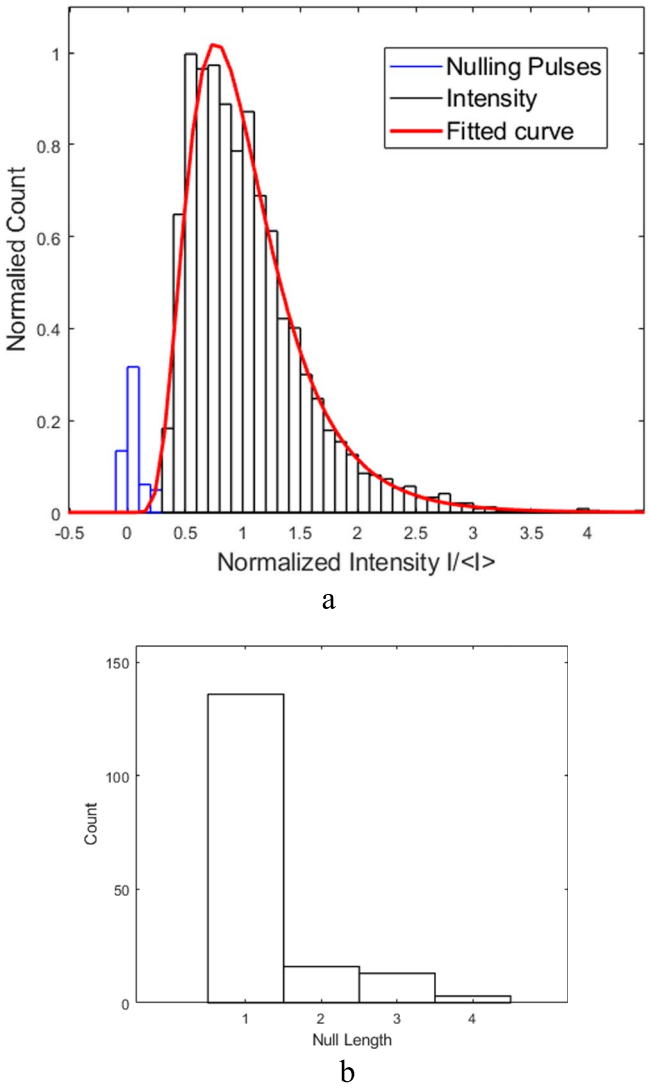

Figure 8. (a) Intensity distribution of pulsar PSR B1237+25. The x-axis is the normalized intensity with respect to the mean $<I>$. The bins marked with blue are the nulling pulses. The pulses with negative intensities are caused by a bad baseline. The total intensity is a log-normal distribution. (b) Null length distribution of the nulling pulses which are pseudo ones lasting for only a few pulses.

with the result of Hankins who reported a width of 2°.6 and Srostlik's (Srostlik & Rankin 2005) who gave a width of 2°.5. These observations suggest that the core width is approximately frequency independent and in favor of the core actually being a central beam cone. By fitting with a five-component Gaussian function, we obtain the full width at half maximum (FWHM) of the core component in flare normal mode of 2°.3.

Due to the aberration and retardation, the radiation emitted from higher altitude will shift to an earlier longitude. The phase shift η_i for each cone can be calculated by the position of the two corresponding components (Gupta & Gangadhara 2003). Here we derive the value of $-0°.80$ for the outer cone and $-0°.36$ for the inner cone. Compared with the result of -0.49 and -0.38 given by Srostlik at 327 MHz for the outer and inner cone respectively, the phase shift of the outer cone is much larger but the inner cone is smaller.

We have noticed that there exists a clear PA jump in the integrated profiles. An analysis has been performed by Smith et al. (2013) to investigate the segregated modes. They applied a three-way OPM segregation method (Deshpande & Rankin 2001) to separate the pulse sequence into three OPMs: a primary polarization mode (PPM), a secondary polarization mode (SPM) and an unpolarized mode. In their result, the PPM usually can be seen in all components, but the SPM almost exists only in components 1, 3 and 5. The SPM seems to be invariant while the mode shifts. Generally, the pulses are dominated by PPM. This result gives a hint that the SPM may be caused by the emissions emitted from a different structure than the PPM modes. In our result, the two cones in normal mode are likely to be dominated by the primary polarization mode, and in the flare normal mode, the core region is dominated by a mode that is different from the cones, and components 4 and 5 are enhanced. For the abnormal mode, the core region is strongly dominated by the SPM, and the PPM of components 4 and 5 are weakened, leading to the PA jumping in the longitude window.

5.2. Modulation Analysis

The 2.8-period modulation of the outer conal component has been reported several times, but little attention was paid to the co-modulation between the core region and the outer cone. Srostlik performed a longitude resolved fluctuation spectral analysis on this pulsar, pointing out that apart from the bright $0.35c/P_1$ modulation, there exists a broader response with P_3 of about $4P_1$ on components 1, 2 and 5 (Srostlik & Rankin 2005). They also argued that there exist two features in the core and the two inner conal components, corresponding to a P_3 of some $37P_1$ and its adjacent response which is approximately twice this value. Although they concluded that the low-frequency feature represents the amplitude modulation of the quasi-periodic flare-normal-mode apparitions, it still remains obscure how those components interact and whether the outer conal components participate in this modulation. It is possible that this longer period modulation is actually an appearance of interaction among all five components. We performed a longitude resolved frequency spectral analysis, and the result shows that the 27-period modulation exists in both the core component and the inner edge of the outer cone component (Figure 10), which reveals that the quasi-periodic modulation in the PS diagram is not just a visual effect, but a real one.

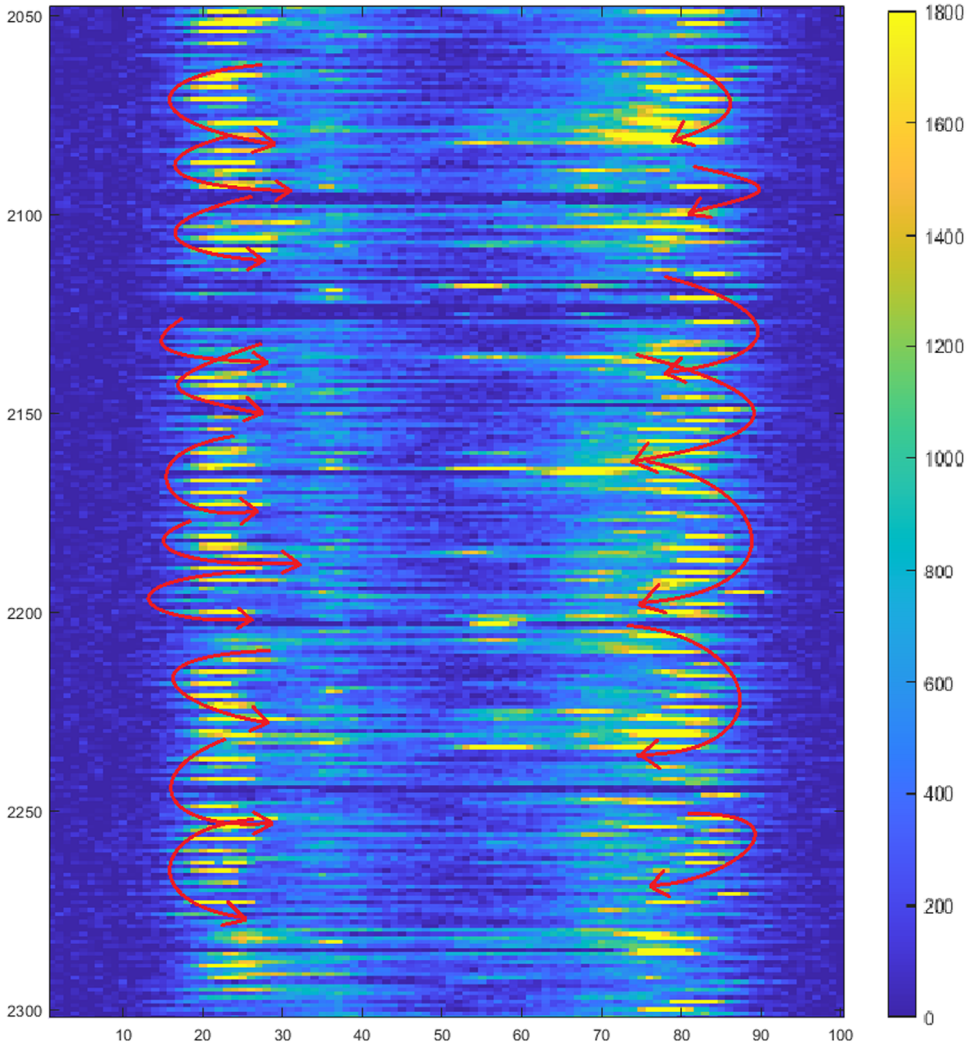

Figure 9. The zoomed-in PS diagram of PSR B1237+25, displaying the pulses in the sequence range between 2050 and 2300. The red arrows show the intensity drift direction of components 1 and 5. The "wave-like" pattern is highly unstable, and sometimes discontinuous. The flare normal mode pulses usually occur around the end of the wave node. Some pseudo null might also occur around the end of the wave nodes.

Though there are no widely accepted criteria for drifting subpulse classification, the drifting subpulses still can be generally divided into two categories: coherent modulated drifting subpulses and diffused modulated drifting subpulses (Basu et al. 2019). Usually, the P_2 and P_3 of the coherent modulated drifting subpulses are stable, while the diffused modulation is sometimes varying. Some of the coherent modulated drifting pulsars have mode changing phenomena too (Weight & Brown 2013; Basu & Mitra 2018), and those different modes have different P_3. The diffused modulated drifting subpulses often manifest a quite different appearances in that the subpulses generally drift randomly in the pulse window. In our case, the "wave-like" modulation may be categorized as a diffused modulated drifting subpulse. The drifting direction is unstable in the longitude direction, and the period of this modulation varies in a large range.

The correlation between different components is depicted in Figure 11. The negative correlation on both sides of the fifth component implies that the peak of the fifth component is actually "wandering" in the longitude window. We took the method (Rankin et al. 2008) to check if those are coherent drifting phenomena and the result excluded such a possibility. Also, we find that the core region has a positive correlation with the fourth component and the front region. As the core activity is strongly related to the flare normal mode, it is possible that such a correlation is caused by the mode changing phenomenon or the shift between different polarization modes.

Another possible explanation for this modulation is that the emission cones precess around the magnetic axis. The most

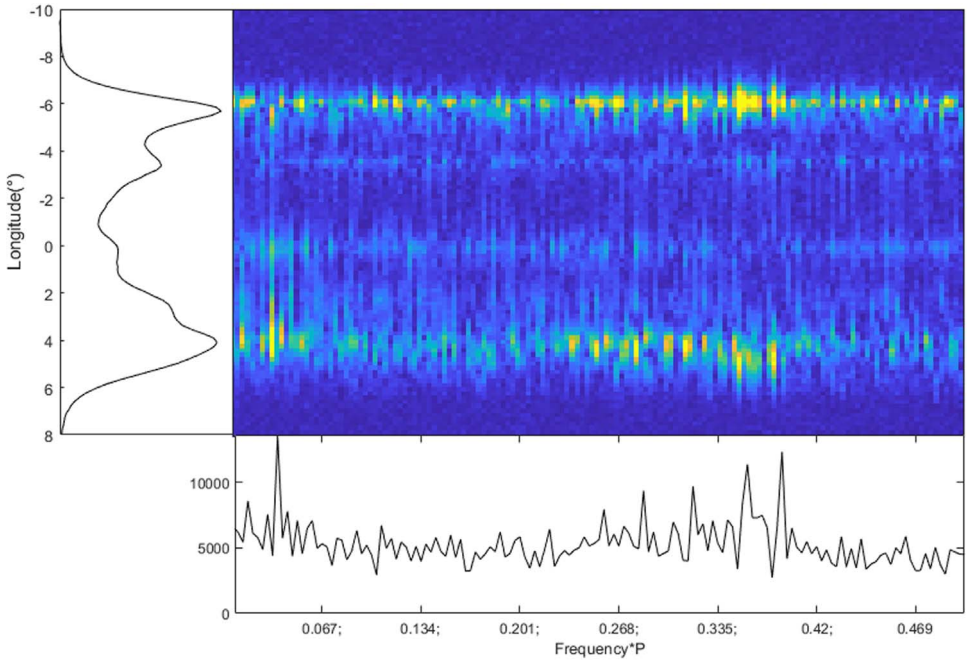

Figure 10. Frequency spectrum of the normal mode of PSR B1237+25. This spectrum consists of 300 pulses. A peak arises at $0.037c/P_1$, corresponding to the 27-period quasi-periodic modulation at the outer cones. The high-resolution spectrum in longitude reveals that the 2.8-period modulation happens on the outer edge of the conal components, while the 27-period modulation takes place on the inner edge of the conal component. The core also shows a slight peak of 27-period modulation.

commonly used model for drifting subpulse is the carousel model. It describes a series of sparks circulating around the magnetic axis, causing a coherent modulated drifting pattern. In earlier studies (Taylor & Huguenin 1971), it had been suggested that the 2.8-period subpulse modulation is caused by the carousel sparks rotating around the magnetic axis, and the subpulses first appear in component 1, and then in component 5. Indeed, the rotation of emission cones can interpret the coherent modulated drifting subpulses, but it is hard to give a proper interpretation to the mode shifting. Dyks (2021) argues that the drifting subpulses can be present when a specially shaped emission region goes around the magnetic axis, but they did not give the prediction of the "wave-like" pattern. They claimed that the flare normal mode is caused by the combined action of the rotation of the emission region itself and the rotation of the emission region that goes around the magnetic axis.

We favor the idea that the emission cones are going around the magnetic axis because it might be the reason for the mode changing and the formation of the wave-like pattern. The current model suggests that, due to the "$E \times B$" in the magnetosphere, the discharging point will rotate in the magnetosphere. But the rotation tracks of the discharging points are not necessarily closed, because the magnetic field on the surface of the neutron star is not perfectly dipole shaped. Considering the collective movement of the discharging point, it is possible that the axis of emission cones does not coincide with the magnetic axis, and precesses around it. Such precession invokes a possible explanation of the "wave-like" pattern. The emission components in the pulses are the endpoint of the secant line of the emission cone. While the emission cones precess around the magnetic axis, the length and the intersection point of the secant on the sightline will change according to the phase of the precession. By recording those points in the sequence diagram, the outer cone components will form a wave-like pattern. Since the magnetosphere usually evolves over time, it is understandable that the "waves" are discontinuous.

The precession can also be used to explain the occurrence of the flare normal mode and the pseudo nulls in the flare normal mode. When the cone precesses near the position that the cones are almost tangent with the sightline, the two secant points will be connected by the emission cone, and thus the flare normal mode forms, and when the emission circle "precesses" to a point that the cones are not crossing with the sightline, the pseudo null will occur. The precession of the emission cones can also be used to explain the periodical nulls.

6. Conclusions

In this paper, we presented a mode changing and modulation analysis of the well-known five-component pulsar B1237+25 which was observed with the FAST facility. We gathered 2605 pulses in one hour of observation at 1.25 GHz with a

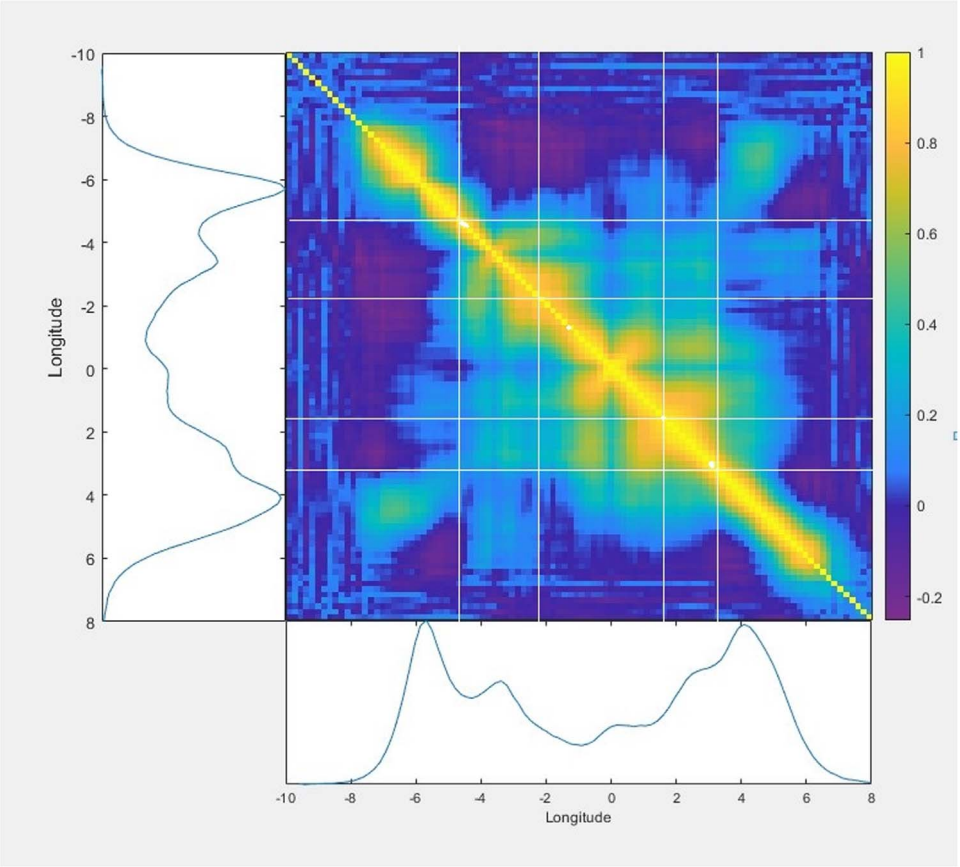

Figure 11. A correlation map of normal mode for PSR B1237+25. To make the correlations between different components clearer, we use white lines to show the boundaries of each component. Component 1 has a weak correlation with the left part of component 5, indicating that the two sides of component 5 are dominated by different emission (propagation) modes. The correlation between the core and the conal component is more evident than in previous studies (Maan & Deshpande 2014).

bandwidth of 400 MHz, and identified three different emission modes. We summarize the findings below:

1. Pulsar B1237+25 exhibits three different emission modes: abnormal mode, quiet normal mode and flare normal mode. The abnormal mode is relatively narrower in longitude, and shows little modulation behavior; the normal mode has a distinctive 2.8-period modulation in the outer conal components.
2. The FAST observation of PSR B1237+25 reveals that the core activity is strongly related to the three distinctive central PA behaviors: the core shows little or no activity in quiet normal mode, but is relatively active in flare normal mode and abnormal mode. The PA "swing" signature is cut off by the core activity, and PA jumping can be found in the abnormal mode. Those evidences affirm that the core is dominated by different polarization modes of the two outer emission cones.
3. Apart from the 2.8-period modulation, there exists a quasi-periodic modulation on the outer conal components. Our observation shows that the outer cone modulation exhibits a "wave-like" modulation, and seems to have some correlation with the core component. The correlation analysis argues that the core has a relation with the inner cone and outer conal components. We discussed the possible origin of such modulation, and conclude that such modulation can be caused by the precession of emission cones around the magnetic axis.

The ultra-high sensitivity of FAST gives us an opportunity to observe the pulsars with unprecedented sensitivity, which enables us to find some subtle structures of emission properties. Those fine structures give us some new evidence to verify current theories and to consummate those theories further.

Acknowledgments

This work is supported by the National Key R&D Program of China under grant number 2018YFA0404703, the Open Project Program of the CAS Key Laboratory of FAST, NAOC,

Chinese Academy of Sciences. This work made use of the data from FAST (Five-hundred-meter Aperture Spherical radio Telescope). FAST is a Chinese national mega-science facility, operated by the National Astronomical Observatories, Chinese Academy of Sciences.

References

Backer, D. C. 1970a, Natur, 228, 42
Backer, D. C. 1970b, Natur, 228, 752
Backer, D. C. 1970c, Natur, 228, 1297
Backer, D. C. 1973, ApJ, 182, 245
Basu, R., & Mitra, D. 2018, MNRAS, 475, 5098
Basu, R., Mitra, D., Melikidze, G. I., et al. 2019, MNRAS, 482, 3757
Deshpande, A. A., & Rankin, J. M. 2001, MNRAS, 322, 438
Dyks, J. 2021, A&A, 653, L3
Force, M. M., & Rankin, J. M. 2010, MNRAS, 406, 237
Gupta, Y., & Gangadhara, R. T. 2003, ApJ, 584, 418
Hankins, T. H., & Wright, G. A. E. 1980, Natur, 288, 18
Herfindal, J. L., & Rankin, J. M. 2007, MNRAS, 380, 430
Hotan, A. W., van Straten, W., & Manchester, R. N. 2004, PASA, 21, 302
Jiang, P., Tang, N. Y., Hou, L. G., et al. 2020, RAA, 20, 064
Lyne, A. G., & Manchester, R. N. 1988, MNRAS, 234, 477
Maan, Y., & Deshpande, A. A. 2014, ApJ, 792, 130
Nan, R. D. 2009, AAS, 41, 474
Qiao, G. J., Lee, K. J., Zhang, B., et al. 2004, ApJ, 616, 127
Qiao, G. J., & Lin, W. P. 1998, A&A, 333, 172
Radhakrishnan, V., & Rankin, J. M. 1990, ApJ, 352, 258
Rankin, J. M. 1983, ApJ, 274, 359
Rankin, J. M. 1986, ApJ, 301, 901
Rankin, J. M. 1990, ApJ, 352, 247
Rankin, J. M., Wright, G. A. E., & Brown, A. M. 2008, MNRAS, 433, 445
Ruderman, M. A., & Sutherland, P. G. 1975, ApJ, 196, 51
Smith, E., Rankin, J. M., & Mitra, D. 2013, MNRAS, 435, 1984
Srostlik, Z., & Rankin, J. M. 2005, MNRAS, 362, 1121
Szary, A., & van Leeuwen, J. 2017, ApJ, 845, 95S
Taylor, J. H., & Huguenin, G. R. 1971, ApJ, 167, 273
van Horn, H. M. 1980, ApJ, 236, 899
van Straten, W., & Bailes, M. 2011, PASA, 28, 1
Wang, Z., Wen, Z. G., Yuan, J. P., et al. 2021, ApJ, 923, 259
Weight, G., & Brown, A. M. 2013, MNRAS, 433, 445
Wen, Z. G., Wang, N., Yuan, J. P., et al. 2016, A&A, 592, 127
Xu, R. X., Liu, J. F., Han, J. L., et al. 2000, ApJ, 535, 354
Yu, Y. Z., Peng, B., Liu, K., et al. 2019, Science China, 62, 959504